J|A|C|S
JOURNAL OF THE AMERICAN CHEMICAL SOCIETY

Article

pubs.acs.org/JACS

Electrochemical Solid-State Phase Transformations of Silver Nanoparticles

Poonam Singh, Kate L. Parent, and Daniel A. Buttry*

Department of Chemistry and Biochemistry, Arizona State University, Tempe, Arizona 85287-1604, United States

S *Supporting Information*

ABSTRACT: Adenosine triphosphate (ATP)-capped silver nanoparticles (ATP−Ag NPs) were synthesized by reduction of $AgNO_3$ with borohydride in water with ATP as a capping ligand. The NPs obtained were characterized using transmission electron microscopy (TEM), UV−vis absorption spectroscopy, X-ray diffraction, and energy-dispersive X-ray analysis. A typical preparation produced ATP−Ag NPs with diameters of 4.5 ± 1.1 nm containing ∼2800 Ag atoms and capped with 250 ATP capping ligands. The negatively charged ATP caps allow NP incorporation into layer-by-layer (LbL) films with poly(diallyldimethylammonium) chloride at thiol-modified Au electrode surfaces. Cyclic voltammetry in a single-layer LbL film of NPs showed a chemically reversible oxidation of Ag NPs to silver halide NPs in aqueous halide solutions and to Ag_2O NPs in aqueous hydroxide solutions. TEM confirmed that this takes place via a redox-driven solid-state phase transformation. The charge for these nontopotactic phase transformations corresponded to a one-electron redox process per Ag atom in the NP, indicating complete oxidation and reduction of all Ag atoms in each NP during the electrochemical phase transformation.

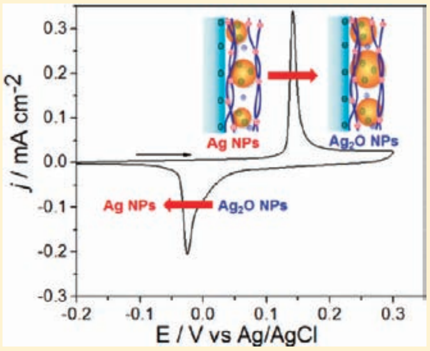

INTRODUCTION

The focus of this report is the characterization of electrochemically driven phase transformations in a new type of water-soluble redox-active silver nanoparticles (Ag NPs) capped by adenosine 5′-triphosphate (ATP, shown in Scheme 1). These NPs are prepared by borohydride reduction of Ag^+ under aqueous conditions in a "one-pot" synthesis and may be purified by selective precipitation, centrifugation, or dialysis followed by isolation as a solid. The synthetic approach is adapted from a previous report describing the synthesis of ATP-capped Au NPs.[1] The solid ATP−Ag NPs may be redissolved in aqueous solution to give stable solutions that can be used to prepare layer-by-layer (LbL) films containing the NPs for electrochemical interrogation. In such films, the Ag NPs can be reversibly electrochemically oxidized to silver halide NPs in halide-containing solutions or Ag_2O NPs in aqueous base. This is significant because these electrochemical processes allow the study of redox-induced solid-state phase transformations in nanoscale materials.

Scheme 1. Structure of ATP^{3-} Showing N7 and the Exocyclic NH_2 Group in Bold

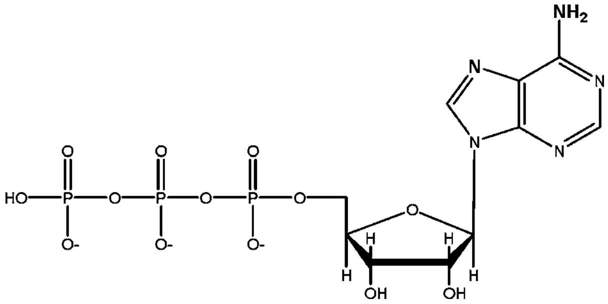

Solid-state phase transformations have recently been a subject of attention since they offer methods to prepare materials, especially nanomaterials, with unique characteristics.[2,3] Two general types of redox-driven phase transformations are topotactic and nontopotactic reactions, in which the structure of the original material is or is not preserved, respectively. Evidence suggests that the use of nanoscale materials can provide pathways to facile, chemically reversible redox reactions for nontopotactic reactions, such as the incorporation of Li into Si to produce $Li_{4.4}Si$, a potential Li battery anode material.[4] One reason for this is the ability of nanoscale materials to accommodate large changes in solid-state molar volumes between the two redox states of the material(s). While there is a large literature on the electrochemical behavior of topotactic solid-state redox transformations, there is much less information available on electrochemically driven solid-state phase transformations for nontopotactic materials. We describe here a new example of a chemically reversible, electrochemical solid-state phase transformation between Ag NPs and either silver halide or silver oxide NPs.

There are several previous reports on the electrochemical behavior of Ag NPs either in thin films or immobilized as

Received: November 21, 2011
Published: March 2, 2012

individual NPs on surfaces. However, for most of those studies, the electrochemical behavior involved either silver oxidation to soluble species [e.g., Ag^+, $AgCl_2^-$, $Ag(NH_3)_3^+$, etc.] or incomplete/irreversible oxidation of the Ag NPs.[5−10] None of the previous cases provided evidence for electrochemically driven solid-state phase transformations. In fact, there are only a few previous examples in which electrochemically driven solid-state phase transformations have been unambiguously demonstrated for any metal particle redox process. Hasse and Scholz used in situ atomic force microscopy (AFM) to follow the electrochemical conversion of an individual silver sulfide crystal to silver metal.[11] They also examined the reduction of an individual PbO nanocrystal to Pb.[12] However, both studies were done with microcrystals having dimensions in the 100−500 nm range, and neither study showed reversible behavior or provided electrochemical charge data that could be used to verify complete redox conversion between the two oxidation states. The present report provides a thorough characterization of the reversible electrochemical transformation of Ag NPs to either silver halide or silver oxide NPs.

■ EXPERIMENTAL SECTION

Synthesis and Purification of ATP−Ag NPs. All chemicals, including $AgNO_3$ (99.999%), ATP disodium salt hydrate (99%), and $NaBH_4$ (99.9%), were purchased from Sigma-Aldrich. Deionized (DI) water of resistivity 18.3 MΩ from a Millipore purification system was used. In a typical synthesis, $AgNO_3$ (10 mM, 3 mL) and ATP (10 mM, 15 mL) were added to 138 mL of DI water in a sealed glass vial under N_2, and the solution was stirred at room temperature for 20 min. Freshly prepared $NaBH_4$ (100 mM, 5 mL) was then quickly added with continued stirring. A light-yellow color appeared immediately upon addition of $NaBH_4$, indicating the formation of Ag NPs. The color of the solution changed gradually from light-yellow to amber over the course of 10 min, after which there was no further color change. The solution was stirred under N_2 for 5 h to allow for any additional growth and capping of the NPs with ATP, finally producing ATP−Ag NPs. Next, the solution was concentrated to 1 mL using a rotary evaporator. Solid NPs were obtained by precipitating the concentrated NPs from solution by repeated addition of small aliquots (in 100 μL increments to a total of 0.5 mL) of isopropanol and were isolated by centrifugation at 1000 rpm for 5 min. The solid NPs may be readily redissolved in water and in aqueous salt solutions. The NPs were further purified by repeated dissolution in water and precipitation using isopropanol. This process was typically repeated five times to eliminate free ATP from the synthetic product as much as possible. This procedure provides ~1 mg of ATP−Ag NPs with a typical yield of 20% based on the metal as the limiting reagent. As described below, the diameter of the NPs produced by this procedure was 4.5 ± 1.1 nm. Variation of the Ag^+:ATP^{3-}:BH_4^- ratio changed the size and polydispersity of the resulting ATP−Ag NPs (to be reported).

Characterization. UV−vis absorption spectra of dilute ATP−Ag NP solutions (0.5 mL of "as prepared" NP solution diluted to 1.2 mL with water) were collected on an Ocean Optics spectrometer (HR4000CG-UV-NIR) in a 1 cm path length, sealed, N_2-purged quartz cuvette. For some of the transmission electron microscopy (TEM) samples, a dilute solution of ATP−Ag NP solution (0.1 mg/mL) was drop-pipetted onto a carbon film supported on a copper grid, and the sample was allowed to dry in air for 30 min. TEM was also used to examine single-layer (1L) LbL samples assembled as described below on Au TEM grids coated with a thin continuous film of Au (Substratek grids, Ted Pella Inc.), which allowed these LbL films to be examined by TEM before and after electrochemical cycling. TEM samples were examined using a Philips CM12S transmission electron microscope operated in bright-field mode at 80 kV. The powder X-ray diffraction (XRD) pattern of solid ATP−Ag NPs was recorded on a Siemens D5000 X-ray diffractometer using Cu Kα radiation at a wavelength of 1.541 Å. Scanning electron microscopy (SEM) was done on an FEI XL30 ESEM-FEG scanning electron microscope. Energy-dispersive X-ray analysis (EDX) was used to obtain the silver to phosphorus atomic ratio for solid NPs. Only Ag and P atomic ratios were analyzed because the low X-ray energies of other elements that were present made their quantitation unreliable. Noncontact AFM (NcAFM) images were obtained on a Veeco CPII scanning probe microscope (SPM) using phosphorus-doped silicon cantilevers (Veeco, model RTESPA-M) with a force constant of 20−80 N/m. For NcAFM characterization, LbL films were assembled (see below) on single-crystal terraces of Au(111) films on mica that were prepared by flame annealing.[13] This allowed ex situ images to be obtained before and after electrochemical cycling of the films.

Electrochemical Measurements. All of the electrochemical measurements were done using a CHI760C potentiostat. A spiral Pt wire and a Ag/AgCl electrode (saturated with NaCl and isolated from the solution with a porous glass frit) were used as the counter and reference electrodes, respectively. The 2 mm diameter gold electrode was polished with aqueous slurries of 1, 0.3, and 0.05 μm alumina for 10 min each, followed each time by sonication in DI water for 10 min. The electrode was then cycled at 100 mV/s in 0.5 M H_2SO_4 between 0 and 1.43 V for ~10 min until a cyclic voltammogram (CV) characteristic of a clean gold surface was obtained. The gold electrode had a surface roughness of 1.9 ± 0.2 after polishing, as determined by the established method of using the gold oxide reduction charge for surface area calibration.[14] Finally, the gold electrode was rinsed with DI water and dried under N_2. Solutions used for electrochemical measurements were made with DI water and were extensively purged with N_2 gas before use.

LbL Assembly Procedure. An LbL film was used to examine the electrochemical behavior of the ATP−Ag NPs attached on Au electrodes. The LbL film was assembled by the following procedure, based loosely on a previously reported method for immobilizing a negatively charged MnO_2 nanoparticle colloid on Au electrodes.[15] The clean gold electrode was dipped in a 10 mM solution of 3-mercaptopropionic acid in ethanol for 60 min to create a self-assembled monolayer and then rinsed in ethanol and dried under N_2. The carboxylic acid groups were deprotonated by placing the electrode into a 0.1 M NaOH solution for 5 min, producing a negatively charged surface. The modified Au electrode was removed from the NaOH solution and immediately placed in a solution of 2 mg/mL poly(diallyldimethylammonium) hydrochloride (PDDA) in 0.1 M NaOH (pH ~12) for 30 min. This produced the first layer of electrostatically adsorbed cationic polymer. The electrode was then washed by dipping it into DI water for 1 min. To immobilize a layer of the anionic ATP−Ag NPs, the electrode was then placed into a 1 mg/mL ATP−Ag NP solution that had been filtered through both 0.1 μm polycarbonate and 20 nm Millex VV sterile Millipore filters. The electrode was left in the NP solution for 30 min to allow time for the NPs to attach to the cationic polymer-modified surface. Again, the electrode was rinsed with DI water and placed into the PDDA solution for 30 min, after which it was rinsed again in DI water for 1 min and dried under N_2 for 1 h. In this way, a 1L LbL film with PDDA termination was created on the gold electrode. The electrode for control experiments was made in a similar way, except that the treatment was stopped after the first PDDA layer (i.e., no NPs were attached to the polymer film). For LbL films on Au-coated TEM grids, the solution concentrations of PDDA and the ATP−Ag NPs were decreased to 1 mg/mL and 0.5 mg/mL, respectively, and the time of exposure to these solutions was also decreased to 15 min each. These changes were made to produce lower NP coverages to facilitate the imaging.

LbL Film on an ITO Substrate. The objective of these measurements was to determine the fate of the ATP capping agent after the electrochemically induced redox transformation from Ag NPs to AgCl (or Ag_2O) NPs and back. For SEM−EDX analysis of the silver to phosphorus ratio in the LbL films, thicker films were required in order to provide adequate X-ray signal intensity. Thus, to create a seven-layer (7L) LbL film on indium tin oxide (ITO), we employed a procedure similar to that described above, except for the initial thiol treatment. Instead, to generate the initial negatively charged surface, the ITO slides were soaked in a 0.1 M NaOH solution for 5 min. This was followed by a PDDA treatment as described above. Following the PDDA treatment, the ITO slide was alternately exposed to the ATP−Ag NP solution and the PDDA solution. This treatment was repeated seven times (with rinsing after each step) to give a 7L LbL film. Afterward, the modified ITO slide was dried overnight under N_2 and analyzed by SEM−EDX to obtain the silver to phosphorus ratio. Next, the slide was electrochemically cycled in 0.5 M NaCl (or 0.1 M NaOH) to oxidize the ATP−Ag NPs to AgCl (or Ag_2O) and then back to Ag (see below). After the slide was cycled in chloride (or hydroxide), SEM−EDX was again used to obtain the silver to phosphorus ratio.

■ RESULTS

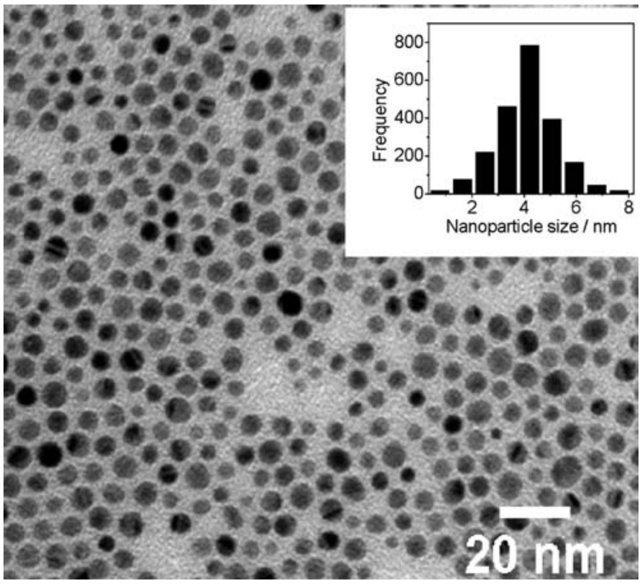

Figure 1. TEM image and (inset) histogram of ATP−Ag NPs. The histogram shows a narrow size distribution of 4.5 ± 1.1 nm (N = 2176).

Characterization of the ATP−Ag NPs using TEM on standard grids (Figure 1) gave a size distribution with an average diameter of 4.5 ± 1.1 nm (number of NPs analyzed, N, was 2176), consistent with the UV−vis and XRD results. There was no evidence for aggregation in numerous TEM images for many such samples. The distinctive contrast that appeared as dark and bright stripes or half-moon shapes in several of the NPs revealed the polycrystalline nature of some of the NPs. This is in accord with past observations of multiply twinned structures for Ag NPs.[16] High-resolution TEM images clearly showed lattice fringes with multiple orientations in individual NPs, as expected for such a case (data not shown). The UV−vis absorption spectrum (Figure S1 in the Supporting Information) of a diluted solution of the ATP−Ag NPs in the "as prepared" form (i.e., the diluted synthesis solution) shows a surface plasmon band with λ_{max} = 400 nm. The band has a shape and center wavelength consistent with 4−7 nm diameter Ag NPs.[17−19] This range is suggested from the data because smaller diameter Ag NPs exhibit a broader band with a low energy tail while larger diameter NPs exhibit a significantly red-shifted λ_{max}.[17] The slight asymmetry in the shape of the plasmon band likely derives from the size distribution. The lack of additional red-shifted peaks indicates the absence of any substantial aggregation, such as dimers or trimers.[20,21] The XRD pattern of the solid NPs (Figure S2) verified the face-centered cubic structure of Ag in the NPs.[22] The average NP size estimated from the width of the XRD peaks using the Debye−Scherrer method was 5 nm.

SEM−EDX has previously been used to obtain quantitative information on NP elemental compositions in Pt−Au nanostructured catalysts.[23] In the present case, the same approach was used to obtain elemental analysis on purified, solid ATP−Ag NP powder samples. Figure S3 shows a representative EDX spectrum. Analysis gave a Ag to P atomic ratio of 3.69. In view of the large depth of penetration of the electron beam in this case (>0.2 μm), these atomic ratios are assumed to give an accurate representation of the average elemental composition of the NP powder. On the basis of a geometrical and density-based estimate of the number of Ag atoms in a 4.5 nm diameter Ag NP (i.e., ~2800 atoms), the number of phosphorus atoms per NP was found to be ~750. This implies ~250 capping ATP ligands per NP (assuming minimal hydrolysis of the ATP phosphate groups during synthesis and handling). This gives an average area of ~0.25 nm^2 per ATP adsorbed on the NP surface, which suggests a perpendicular orientation of ATP that is consistent with a relatively close-packed structure. Previous scanning tunneling microscopy and electrochemical studies of adenine adsorption on Au(111) and Hg suggested close-packed molecular areas of 0.24 and 0.40 nm^2, respectively, in reasonable support of the present interpretation.[24,25] This picture of the adsorbed ATP species is also in agreement with a previous Raman study of the adsorption of adenine and its derivatives at silver colloid surfaces, which showed the adsorption to be end-on with interactions between the metal surface and both the N7 heterocyclic nitrogen and the adjacent exocyclic NH_2 group (see Scheme 1).[26] Bidentate binding of the adenine headgroup with the phosphate groups pointed away from the surface would generate both stable capping and a highly negatively charged NP surface that would lead to large interparticle repulsions, consistent with the remarkable stability of these NPs against aggregation both in solution and when isolated as a solid.

A convenient method for examining the electrochemical behavior of NPs involves their immobilization in LbL films on electrode surfaces.[27−30] This approach was used here to probe both the double-layer charging of ATP−Ag NPs in LbL films and their oxidation to Ag(I) and rereduction to Ag(0) under various conditions. Figure 2 compares CVs showing double-layer charging behavior for a control film (i.e., an anchor layer but no NPs; see the Experimental Section) and a 1L LbL film on a gold electrode in 0.1 M NaOH. The scan was limited to a small potential range in which no Ag(I)/Ag(0) redox behavior would be observed (see below). The increase in the double-

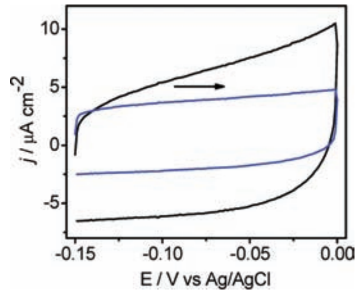

Figure 2. CVs showing the double-layer charging behavior of control (blue) and 1L LbL (black) films of ATP−Ag NPs in 0.1 M NaOH under a N_2 saturated atmosphere. Scan rate: 50 mV/s.

layer charging envelope for a 1L LbL film relative to the control film confirms that charging current flows to equilibrate the NPs with the potential of the underlying electrode. This type of charging for immobilized NPs has been observed in previous instances.[27−29] In the present case, the double-layer charging appears as a continuous featureless process, since these NPs are too polydisperse and too large to exhibit discrete, quantized charging effects.[19,31]

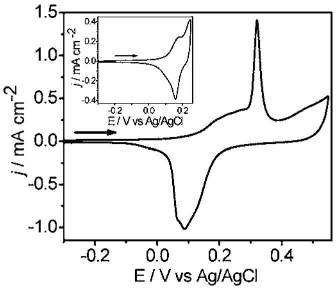

Figure 3. CV of a 1L LbL film of ATP−Ag NPs in N_2-saturated 0.1 M NaOH, showing the monolayer oxidation plus the first bulk oxidation of Ag NPs. The inset shows the monolayer oxidation of the 1L LbL film in 0.1 M NaOH. Scan rate: 50 mV/s.

The electrochemical behavior of the Ag NPs in hydroxide solution was also examined over a wider potential range encompassing Ag oxidation. Figure 3 shows the CV of a 1L LbL film of ATP−Ag NPs in aqueous 0.1 M NaOH. The positive scan shows an anodic prewave beginning at +0.1 V followed by a larger anodic peak centered at +0.32 V. During the negative scan, a cathodic process with multiple peaks centered at +0.1 V is observed. The inset shows a scan limited to the region of the prewave, which reveals an anodic peak at +0.13 V and its corresponding cathodic peak also at +0.13 V. By analogy to past discussions of silver oxide formation on bulk silver electrodes, the main anodic peak at +0.32 V is attributed to electrooxidation of Ag in the Ag NPs to Ag_2O, and the cathodic peak at +0.1 V is attributed to the reverse of this process. The apparent formal potential for the Ag/Ag_2O redox couple of ca. +0.2 V (the average of the anodic and cathodic peak potentials) is in reasonable agreement with the E_0 value of +0.12 V vs Ag/AgCl reported for the bulk material.[32] On the basis of reports for bulk silver electrodes, the prewave is attributed to reversible surface oxidation of the NPs prior to their "bulk" oxidation.[33−38] The anodic and cathodic charges for the entire oxidation and reduction processes (i.e., including both the prewave and main wave) have identical values of 1.47×10^{-3} C cm^{-2}. Thus, the charge efficiency for the redox conversion shown in Figure 3 is 100%. On the basis of a diameter of 4.5 nm and the assumption that the Ag in the NPs is completely oxidized to Ag(I) during the anodic scan (see below), this charge is consistent with an NP surface coverage of 3.3×10^{12} NPs cm^{-2}. This can be compared to the coverage expected for a close-packed layer of NPs. Using a diameter of 4.5 nm and the two-dimensional fill factor of 0.91 for hexagonal close packing of spheres, one obtains 5.7×10^{12} NPs cm^{-2}. Thus, if oxidation of the NPs is assumed to be complete, the experimental charge suggests a surface coverage of NPs of ~58% of a close-packed layer. We return below to the issue of what fraction of the Ag atoms in the NPs undergo redox transformation during the anodic and cathodic redox processes.

A key question is whether the redox process shown in Figure 3 corresponds to a direct solid-state conversion of Ag to Ag_2O for each individual NP or if the conversion process is mediated somehow through soluble silver species (i.e., whether the NPs retain their individual identities or exchange material via dissolution/redeposition processes during the redox cycle). To address this, both TEM and AFM were used to examine 1L LbL films before and after electrochemical cycling. Figure 4 shows TEM images of a 1L LbL film on a thin-film Au TEM grid (a) before and (b) after cycling in 0.1 M NaOH. These TEM grids are characterized by very thin regions of Au (lighter contrast) connecting slightly thicker regions (darker contrast), with the average Au film thickness of 2 nm. Figure S4 shows a TEM image of a virgin grid. In Figure 4a, the individual ATP−Ag NPs can be seen in the initially formed LbL film, which spans both the thin and thick regions of the Au film. Figure 4b shows the same film after a scan across the Ag/Ag_2O redox process and back (under the same conditions as Figure 3). Figure S5 is a TEM image of a similar film in the Ag_2O state (i.e., after oxidation but before reduction back to Ag) that shows the discrete nature of the Ag_2O NPs in this film. These TEM images provide unambiguous evidence that the NPs retain their individual identities during the scan. This confirms that during the scan they are converted directly from Ag to Ag_2O and back in a solid-state phase transformation, as dissolution and redeposition mediated through solution-phase species would lead to Ostwald ripening and particle coarsening.[39]

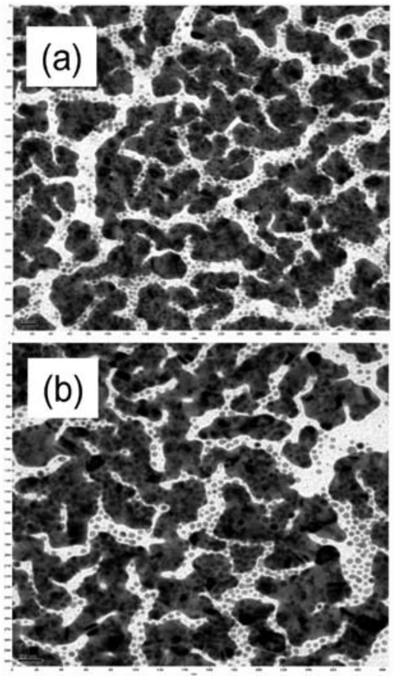

Figure 4. TEM images of a 1L LbL film of ATP−Ag NPs (a) before and (b) after cycling once over the Ag oxidation waves in N_2-saturated 0.1 M NaOH over a potential range of −0.1 to +0.4 V. Scan rate: 50 mV/s.

AFM was also used to examine the NPs before and after redox cycling. Figure 5 shows AFM images of a 1L LbL film on a single-crystal terraced Au(111) electrode that were obtained before and after electrochemical cycling in 0.1 M NaOH. Figure 5a shows the image before cycling, and Figure 5b shows a higher-magnification image of the selected area. Height measurements of isolated NPs cast from solution onto highly

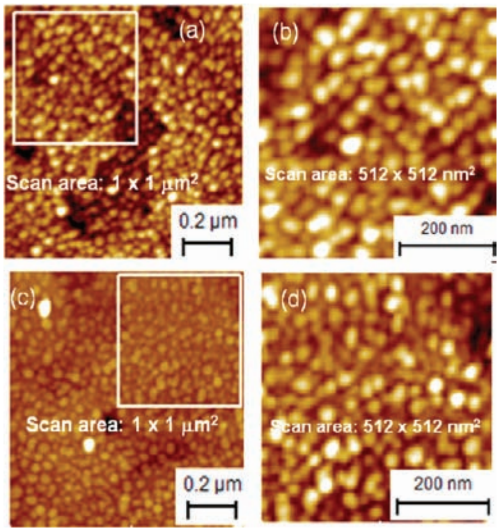

Figure 5. NcAFM image of a 1L LbL film of ATP−Ag NPs (a) before and (c) after scanning for a cycle in N_2-saturated 0.1 M NaOH over a potential range of +0.42 V at a scan rate of 50 mV/s. (b, d) Zoomed images of the square areas marked in (a) and (c), respectively.

oriented pyrolytic graphite were found to be in good agreement with the TEM-based diameter of 4.5 nm (data not shown). However, for such small NPs, quantitative AFM measurements of the diameter and interparticle spacing from lateral distances are not reliable because of convolution of the NP diameter with the radius of curvature of the tip.[40,41] Nevertheless, the image gives a sense of the homogeneity and surface coverage of the NPs in the film and is similar to images from past reports of LbL films containing Ag NPs of various types.[10,42] Figure 5c shows an image of the same film after cycling through the Ag/Ag_2O redox process under the same conditions as in Figure 3, and Figure 5d shows a higher magnification image of the selected area. As for the TEM images above, these images confirm that the NPs retained their size and lateral distribution after redox cycling, consistent with a phase transformation from Ag to Ag_2O and back for individual NPs.

Chemically reversible oxidation and reduction of the ATP−Ag NPs were also observed in halide solutions. Figure 6 shows CVs of 1L LbL films in three NaCl solutions having different concentrations, with $NaNO_3$ added to maintain a sufficient electrolyte concentration. In each solution, one observes an oxidation peak and the corresponding reduction peak. These are attributed to oxidation of Ag to AgCl and reduction of AgCl back to Ag, respectively. Linear plots of the anodic and cathodic peak potentials versus log [Cl^-] had slopes of 54 and 57 mV per decade, respectively. This demonstrates a Nernstian dependence of the electrochemical process on the chloride concentration. The charge efficiency for the oxidation and rereduction in chloride solution was 100% for a given scan, as observed for the Ag/Ag_2O redox transformation discussed above. This suggests that both the oxidized and reduced forms of the NPs are stable and sufficiently insoluble on the time scale of the experiment to prevent substantial loss of material from the NPs. As for the oxide case, the process shown in Figure 6 is attributed to an electrochemically driven phase transformation of the NPs from Ag to AgCl and back. This is supported by the TEM images in Figures S6 and S7, which show the film in the AgCl state and after reduction back to the Ag state, respectively. As for the oxide case, we see preservation of the NP identities and sizes after redox cycling. This cyclic process between Ag and AgCl is analogous to the redox-driven solid-state phase transformation of Ag NPs to AgCl NPs speculatively assigned by Ting et al.[9] in an amplified bioanalytical scheme.

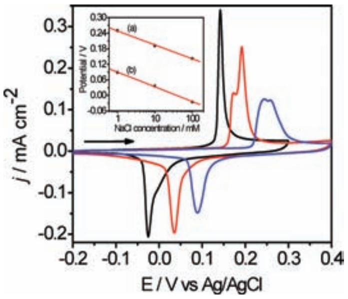

Figure 6. CVs of 1L LbL films of ATP−Ag NPs in N_2-saturated solutions having different concentrations of NaCl [100 mM (black), 10 mM (red), and 1 mM (blue)], all containing 0.1 M $NaNO_3$ as an electrolyte. Scan rate: 10 mV/s. The inset shows the linear-fit plots of the (a) oxidation and (b) reduction potentials at different NaCl concentrations.

The electrochemical behavior in other halide solutions was also examined. Figure 7 shows CVs for a 1L LbL film sequentially scanned in solutions of 0.05 M NaCl, 0.05 M NaBr, 0.05 M NaI, and 0.1 M NaOH. This set of CVs shows that the oxidation potential for the Ag NPs shifts as expected when different halides are present, according to the $E°$ values of 0.00, −0.15, and −0.37 V vs Ag/AgCl for the Ag/AgCl, Ag/AgBr, and Ag/AgI redox couples, respectively.[32] In all cases, the charge efficiency for the oxidation and subsequent reduction was near 100%, suggesting reversible conversion of the Ag NPs to the silver halide or silver oxide phase during the anodic scan and subsequent conversion back to Ag during the cathodic scan. Table 1 gives the charges for oxidation of the Ag NPs to the various silver halides as well as to Ag_2O. Essentially identical charges were observed for all of the oxidations. This is consistent with complete oxidation of the Ag NPs in the LbL

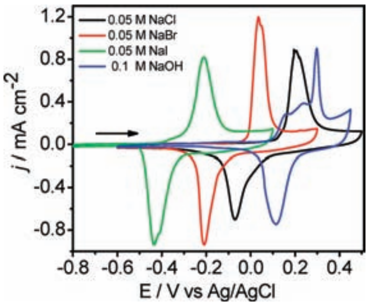

Figure 7. CVs of a 1L LbL film of ATP−Ag NPs in N_2-saturated 0.05 M NaCl, NaBr, NaI, and NaOH solutions. Scan rate: 50 mV/s.

Table 1. Anodic Oxidation Charges for a 1L LbL Film in Different Redox Transformations

phase transformation	charge (mC/cm^2)
Ag/AgCl	1.24
Ag/AgBr	1.26
Ag/AgI	1.27
Ag/Ag_2O	1.23

film to the various halide or oxide forms during the phase transformation, since incomplete oxidation (e.g., creation of a core−shell structure) would almost certainly lead to differences in the oxidation charges for the various conditions.

An additional question concerns whether the NPs retain their ATP capping ligands during the redox cycling shown in Figures 3, 6, and 7. To address this, SEM−EDX was used to assay the P/Ag ratio after cycling in 0.5 M NaCl for a thicker (7L) LbL film on an ITO substrate. The EDX spectrum for this film (Figure S4) showed complete loss of the P signal at 2.0 keV after a single cycle, confirming the removal of all of the ATP capping ligands during the electrochemical phase transformation. The same loss of the P signal was observed when the ATP−Ag NPs were oxidized in aqueous base. It is interesting that even though the capping ligands are lost during redox cycling, the NPs do not appear to desorb from the LbL film or aggregate. This could be due to their entrapment in the PDDA polymer layer used to stabilize the LbL film or to NP aggregation within the film after loss of the capping ligands. Aggregation would be possible only in cases where NPs were in sufficient proximity and thus would not be expected for a case such as that shown in the TEM images in Figure 4, where the NPs are substantially separated. For the halide cases, it is also possible that the surface charge on the "bare" NPs remained negative in both the silver and silver halide states, since the experiment was conducted in a solution containing the halide, which should have been strongly adsorbed on both surfaces.[43−48] This would maintain the favorable electrostatic interactions between the anionic NPs and the cationic PDDA polymer that drive film formation and stability. Thus, loss of the ATP capping ligands may not be expected to cause NP loss from the LbL film under these conditions.

Finally, the generation of higher oxidation states of Ag at higher potentials was examined. Figure 8 shows a CV of a 1L LbL film in NaOH solution over an extended positive potential range up to +0.8 V. After the Ag_2O oxidation, a second process with an anodic peak at +0.68 V was observed. On the basis of previous studies, this is attributed to oxidation to "AgO",[49,50] which is known to resemble a solid-state mixture of Ag(I) and Ag(III).[51] AFM images of the surface showed that the film was significantly damaged following scans into this potential range (data not shown). This is likely due to a combination of oxidative instability of the thiol monolayer used to anchor the LbL film at the Au surface and bulk oxidation of Au. Thus, this redox process was not investigated further.

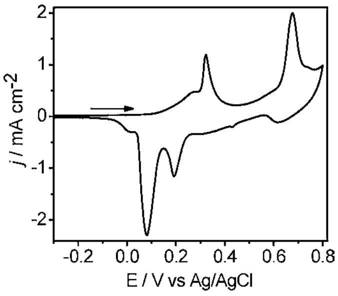

Figure 8. CV of a 1L LbL film of ATP−Ag NPs in N_2-saturated 0.1 M NaOH, showing the first and second bulk oxidations of the Ag NPs. Scan rate: 50 mV/s.

■ DISCUSSION

These results demonstrate the chemically reversible, electrochemically driven solid-state phase transformation of Ag NPs to either Ag_2O or silver halide phases. They can be considered in the context of past studies of formation of silver oxides and silver halides on Ag electrodes and Ag particles.[37,49,52−57] In the case of silver oxide, several mechanisms for the oxidation have been proposed. In some cases, growth of silver oxide at silver electrode surfaces has been postulated to occur through dissolution and redeposition of soluble species.[58] Other workers have described redox cycling between silver and silver oxide in NPs and nanostructured materials without mention of soluble species.[49,53] Still others have described mixed behavior for silver oxide growth at silver surfaces, in which solid-state phase transformations occur under some conditions while dissolution and redeposition via a nucleation and growth mechanism occur under other conditions.[52,59] In the present case, it is clear from the TEM images of Ag NPs in the LbL film before and after redox cycling that the redox process is a solid-state phase transformation, since dissolution/redeposition processes would lead to coarsening.

The case for silver halides is similar to that for oxidation of Ag NPs to Ag_2O NPs. Under some conditions, oxidation can lead to soluble silver species. This can occur (1) when the rate of the oxidation process [i.e., generation of Ag(I)] exceeds the rate of delivery of the halide to the surface by diffusion[57] or (2) when the concentration of the halide is sufficiently high to drive the formation of soluble species (e.g., $AgCl_2^-$ or AgI_2^-) by dissolution of the solid silver halide.[60] Previous studies have demonstrated both types of behavior. When neither of these conditions prevails, one can observe direct conversion of Ag to the silver halide phase, such as that reported for oxidation of silver surfaces to produce AgCl and AgBr.[55,61] Direct solid-state electrochemical conversion of Ag_2S to Ag has also been observed using in situ AFM, though reversibility was not demonstrated.[11] In the present case, the conditions were chosen to favor a direct solid-state phase transformation, bypassing the formation of soluble intermediates.

The CVs in Figures 3, 6, and 7 show large peak separations between the anodic and cathodic peaks. These peak separations increase with increasing scan rate (data not shown), suggesting a kinetic origin. This is likely due to the kinetics for the phase transformation process in these systems, as previously discussed for silver electrooxidation to AgCl at Ag electrode surfaces.[47,55,56] Another interesting issue is whether these systems transform from one phase to another via core−shell structures or via nucleation and growth from a single point on the NP surface. This question was recently addressed in separate discussions of metal core−metal oxide shell materials[62] and topotactic redox phase transformations between $FePO_4$ and $LiFePO_4$.[63] Efforts to address these connected issues are currently underway.

■ CONCLUSIONS

This report has described the first synthesis of ATP-capped Ag NPs. Characterization showed that the synthetic method provides a reasonably monodisperse product with a diameter of 4.5 ± 1.1 nm. SEM−EDX showed that the ATP capping agents are present at high coverage at the surface of the NPs. A roughly perpendicular orientation of the adenosine headgroup at the NP surface is suggested, which is consistent with expectations from previous Raman analysis of adenine adsorption on Ag colloids.[26] Electrochemical data suggested that these Ag NPs can be reversibly oxidized to the respective halide phases in solutions containing Cl^-, Br^-, or I^- as well as to Ag_2O in basic solutions. TEM images showed that these electrochemically driven solid-state phase transformations occur by direct conversion of each NP from silver metal to the silver halide or silver oxide phase and that aggregation does not occur after redox cycling. Size effects of the redox properties for the NPs studied here were not observed, likely because they are too large for such phenomena. Efforts to examine smaller NPs toward that end are underway. Finally, these systems offer the possibility of using in situ TEM to image the solid-state phase transformation directly, an experiment that seems feasible with new in situ TEM methods.[64]

■ ASSOCIATED CONTENT

Ⓢ Supporting Information

UV−vis spectra, XRD diffraction data, additional TEM images, and EDS spectra. This material is available free of charge via the Internet at http://pubs.acs.org.

■ AUTHOR INFORMATION

Corresponding Author

Dan.Buttry@asu.edu

Notes

The authors declare no competing financial interest.

■ ACKNOWLEDGMENTS

We thank the electron microscopy laboratory in the ASU School of Life Sciences Bioimaging Facility for providing access to the TEM facility. This material is based upon work supported by the National Science Foundation under Grant CHE-0957122.

■ REFERENCES

(1) Zhao, W.; Gonzaga, F.; Li, Y.; Brook, M. A. *Adv. Mater.* **2007**, *19*, 1766−1771.

(2) Moon, G. D.; Ko, S.; Xia, Y. N.; Jeong, U. *ACS Nano* **2010**, *4*, 2307−2319.

(3) Muthuswamy, E.; Brock, S. L. *Chem. Commun.* **2011**, *47*, 12334−12336.

(4) Schoen, D. T.; Meister, S.; Peng, H. L.; Chan, C.; Yang, Y.; Cui, Y. *J. Mater. Chem.* **2009**, *19*, 5879−5890.

(5) Branham, M. R.; Douglas, A. D.; Mills, A. J.; Tracy, J. B.; White, P. S.; Murray, R. W. *Langmuir* **2006**, *22*, 11376−11383.

(6) Chaki, N. K.; Sharma, J.; Mandle, A. B.; Mulla, I. S.; Pasricha, R.; Vijayamohanan, K. *Phys. Chem. Chem. Phys.* **2004**, *6*, 1304−1309.

(7) Ivanova, O. S.; Zamborini, F. P. *J. Am. Chem. Soc.* **2010**, *132*, 70−72.

(8) Ng, K. H.; Liu, H.; Penner, R. M. *Langmuir* **2000**, *16*, 4016−4023.

(9) Ting, B. P.; Zhang, J.; Khan, M.; Yang, Y. Y.; Ying, J. Y. *Chem. Commun.* **2009**, 6231−6233.

(10) Zhao, S.; Zhang, K.; An, J.; Sun, Y. Y.; Sun, C. Q. *Mater. Lett.* **2006**, *60*, 1215−1218.

(11) Hasse, U.; Scholz, F. *Electrochem. Commun.* **2005**, *7*, 173−176.

(12) Hasse, U.; Scholz, F. *Electrochem. Commun.* **2001**, *3*, 429−434.

(13) Tang, L.; Han, B.; Persson, K.; Friesen, C.; He, T.; Sieradzki, K.; Ceder, G. *J. Am. Chem. Soc.* **2010**, *132*, 596−600.

(14) Hvastkovs, E. G.; Buttry, D. A. *Langmuir* **2006**, *22*, 10821−10829.

(15) Lvov, Y.; Munge, B.; Giraldo, O.; Ichinose, I.; Suib, S. L.; Rusling, J. F. *Langmuir* **2000**, *16*, 8850−8857.

(16) Marks, L. D. *Rep. Prog. Phys.* **1994**, *57*, 603−649.

(17) Slistan-Grijalva, A.; Herrera-Urbina, R.; Rivas-Silva, J. F.; Avalos-Borja, M.; Castillon-Barraza, F. F.; Posada-Amarillas, A. *Physica E* **2005**, *27*, 104−112.

(18) Mulvaney, P. *Langmuir* **1996**, *12*, 788−800.

(19) Ung, T.; Giersig, M.; Dunstan, D.; Mulvaney, P. *Langmuir* **1997**, *13*, 1773−1782.

(20) Chen, G.; Wang, Y.; Tan, L. H.; Yang, M. X.; Tan, L. S.; Chen, Y.; Chen, H. Y. *J. Am. Chem. Soc.* **2009**, *131*, 4218−4219.

(21) Li, W. Y.; Camargo, P. H. C.; Lu, X. M.; Xia, Y. N. *Nano Lett.* **2009**, *9*, 485−490.

(22) Liu, X. H.; Luo, J.; Zhu, J. *Nano Lett.* **2006**, *6*, 408−412.

(23) Hu, Y. J.; Zhang, H.; Wu, P.; Zhou, B.; Cai, C. X. *Phys. Chem. Chem. Phys.* **2011**, *13*, 4083−4094.

(24) Prado, C.; Prieto, F.; Rueda, M.; Feliu, J.; Aldaz, A. *Electrochim. Acta* **2007**, *52*, 3168−3180.

(25) Tao, N. J.; Derose, J. A.; Lindsay, S. M. *J. Phys. Chem.* **1993**, *97*, 910−919.

(26) Giese, B.; McNaughton, D. *J. Phys. Chem. B* **2002**, *106*, 101−112.

(27) Uosaki, K.; Kondo, T.; Okamura, M.; Song, W. B. *Faraday Discuss.* **2002**, *121*, 373−389.

(28) Zamborini, F. P.; Hicks, J. F.; Murray, R. W. *J. Am. Chem. Soc.* **2000**, *122*, 4514−4515.

(29) Benedetti, T. M.; Bazito, F. F. C.; Ponzio, E. A.; Torresi, R. M. *Langmuir* **2008**, *24*, 3602−3610.

(30) Hammond, P. T. *Adv. Mater.* **2004**, *16*, 1271−1293.

(31) Murray, R. W. *Chem. Rev.* **2008**, *108*, 2688−2720.

(32) Bard, A. J.; Parsons, R.; Jordan, J. *Standard Potentials in Aqueous Solution*; Marcel Dekker: New York, 1985.

(33) Ahern, A. J.; Nagle, L. C.; Burke, L. D. *J. Solid State Electrochem.* **2002**, *6*, 451−462.

(34) Tilak, B. V.; Perkins, R. S.; Kozlowska, H. A.; Conway, B. E. *Electrochim. Acta* **1972**, *17*, 1447−1469.

(35) Stonehart, P. *Electrochim. Acta* **1968**, *13*, 1789−1803.

(36) Stonehart, P.; Portante, F. P. *Electrochim. Acta* **1968**, *13*, 1805−1814.

(37) Hur, T. U.; Chung, W. S. *J. Electrochem. Soc.* **2005**, *152*, A179−A185.

(38) Hur, T. U.; Chung, W. S. *J. Electrochem. Soc.* **2005**, *152*, A996−A1000.

(39) Redmond, P. L.; Hallock, A. J.; Brus, L. E. *Nano Lett.* **2005**, *5*, 131−135.

(40) Ramirez-Aguilar, K. A.; Rowlen, K. L. *Langmuir* **1998**, *14*, 2562−2566.

(41) Schwarz, U. D.; Haefke, H.; Reimann, P.; Guntherodt, H. J. *J. Microsc. (Oxford)* **1994**, *173*, 183−197.

(42) Cui, X. Q.; Li, C. M.; Bao, H. F.; Zheng, X. T.; Lu, Z. S. *J. Colloid Interface Sci.* **2008**, *327*, 459−465.

(43) Roy, D.; Furtak, T. E. *J. Electroanal. Chem.* **1987**, *228*, 229−250.

(44) Schmidt, E.; Stucki, S. *J. Electroanal. Chem.* **1973**, *43*, 425−440.

(45) Sneddon, D. D.; Gewirth, A. A. *Surf. Sci.* **1995**, *343*, 185−200.

(46) Valette, G.; Parsons, R. *J. Electroanal. Chem.* **1986**, *204*, 291−297.

(47) Jovic, B. M.; Jovic, V. D.; Drazic, D. M. *J. Electroanal. Chem.* **1995**, *399*, 197−206.

(48) Kallay, N.; Preocanin, T.; Supljika, H. *J. Colloid Interface Sci.* **2008**, *327*, 384−387.

(49) Pan, J. Q.; Sun, Y. Z.; Wang, Z. H.; Wan, P. Y.; Liu, X. G.; Fan, M. H. *J. Mater. Chem.* **2007**, *17*, 4820−4825.

(50) Salvarezza, R. C.; Becerra, J. G.; Arvia, A. J. *Electrochim. Acta* **1988**, *33*, 1753−1759.

(51) McMillan, J. A. *Chem. Rev.* **1962**, *62*, 65−80.

(52) Becerra, J. G.; Salvarezza, R.; Arvia, A. J. *Electrochim. Acta* **1990**, *35*, 595−604.

(53) Ghilane, J.; Fan, F. R. F.; Bard, A. J.; Dunwoody, N. *Nano Lett.* **2007**, *7*, 1406−1412.

(54) Nagle, L. C.; Ahern, A. J.; Burke, L. D. *J. Solid State Electrochem.* **2002**, *6*, 320−330.

(55) Brolo, A. G.; Sharma, S. D. *Electrochim. Acta* **2003**, *48*, 1375–1384.

(56) Demele, M. F. L.; Salvarezza, R. C.; Moll, V. D. V.; Videla, H. A.; Arvia, A. J. *J. Electrochem. Soc.* **1986**, *133*, 746–752.

(57) Hasse, U.; Fletcher, S.; Scholz, F. *J. Solid State Electrochem.* **2006**, *10*, 833–840.

(58) Hepel, M.; Tomkiewicz, M. *J. Electrochem. Soc.* **1984**, *131*, 1288–1294.

(59) Becerra, J. G.; Salvarezza, R. C.; Arvia, A. J. *Electrochim. Acta* **1988**, *33*, 1431–1437.

(60) Birss, V. I.; Wright, G. A. *Electrochim. Acta* **1982**, *27*, 1439–1443.

(61) Hasse, U.; Wagner, K.; Scholz, F. *J. Solid State Electrochem.* **2004**, *8*, 842–853.

(62) Li, W.; Jin, X. B.; Huang, F. L.; Chen, G. Z. *Angew. Chem., Int. Ed.* **2010**, *49*, 3203–3206.

(63) Meethong, N.; Kao, Y. H.; Tang, M.; Huang, H. Y.; Carter, W. C.; Chiang, Y. M. *Chem. Mater.* **2008**, *20*, 6189–6198.

(64) Liu, X. H.; Huang, J. Y. *Energy Environ. Sci.* **2011**, *4*, 3844–3860.